Nanoscale

PAPER

View Article Online
View Journal | View Issue

Cite this: *Nanoscale*, 2023, **15**, 15288

Electronic structure study of dual-doped II–VI semiconductor quantum dots towards single-source white light emission†

Payel Mondal, [a] Sowmeya Sathiyamani,[a] Subham Das [a] and Ranjani Viswanatha *[a,b]

Received 20th July 2023,
Accepted 5th September 2023

DOI: 10.1039/d3nr03542e

rsc.li/nanoscale

Single-source white light emitting colloidal semiconductor quantum dots (QDs) is one of the most exciting and promising high-quality solid-state light sources to meet the current global demand for sustainable resources. While most of the previous methods involve dual (green-red) emissive nanostructures coated on blue LEDs to achieve white light, this work describes a single-source white light emitter of robust and superior quality using dual-doping. A modified synthesis method for intense white light emitting Cu, Mn dual-doped ZnSe QDs is engineered such that the extent of doping and concentration of ligands can alter their electronic structures. This is then customized to obtain various types of white light emissions ranging from warm white to cool white. Further, the composition-driven change in the electronic structure of the host QDs is exploited to achieve emission tunability over the entire visible range.

1. Introduction

Global electricity consumption has continued to rise very fast while the existing renewable sources can fulfill only half of the increasing demand. Thus, the development of promising less power-consuming alternatives became crucial to replace conventional lighting systems. Quantum dots (QDs), also known as colloidal semiconductor nanocrystals (NCs), are potential new-generation nanophosphors for lighting applications due to their controllable bandgap, emission tunability, low-cost synthesis, and high photoluminescence quantum yield (PLQY).[1–5] Recently perovskite QDs have garnered a lot of attention in producing efficient white light emission due to their extremely high PLQY and ease of synthesis.[6–8] However, halide perovskites being ionic in nature are very vulnerable to air, water, *etc.*, and colloidal II–VI semiconductor QDs are preferred due to their more covalent nature. Conventionally, white light was achieved by mixing QDs emitting primary colors or coating green and red phosphors onto blue or ultraviolet LEDs. For example, blue, green, and red-emitting CdZnS alloy, ZnSe/CdSe/ZnS, and CdSe/ZnS core/shell QDs respectively,[9] or different compositions of CdSe/ZnS core/shell QDs were blended together to fabricate white light emitting devices (WLED).[10,11] However, mixing QDs can lead to undesired energy transfers, reabsorption, and unexpected temporal color shift due to the non-uniform stability of QDs leading to reduced luminous efficacy. Thus, single-source emitters with broad emission are preferred over multi-component systems for higher luminous efficacy.

Two ways of achieving single-source emitters for white light have been explored in the literature, namely, the use of trap states and dopant mid-gap states. White light achieved using ill-defined surface states is not robust and hence poorly understood. White light from trap-rich CdSe[12] QDs and onion-like CdSe/ZnS/CdSe/ZnS,[13] and $Zn_{0.93}Cd_{0.07}Se$[14] alloy QDs involved sensitive manipulation of trap states and reaction parameters. Dual-doped QDs like Cu, Mn co-doped Zn–In–S/ZnS core/shell QDs after combining with commercially available GaN blue light emitter with a color rendering index (CRI) as high as 95[15] were reported as alternatives to poorly controlled trap state based white light emitters. In fact, Cu, Mn dual-doped ZnSe NC-system was reported earlier[16] involving trap state contribution to the white light emission and the use of toxic tributylphosphine (TBP) during synthesis. Moreover, the NC system lacks a detailed analysis of the dual-doping and suffers from low PLQY due to the low reactivity of the TBP-Se precursor. Thus, it remains challenging to efficiently incorporate two dopants to obtain robust and stable dual-doped QDs and reliably tune the white light emission with high PLQY.[17] Herein, we devised a new synthetic strategy that overcomes all the problems of previously reported materials.

[a]*New Chemistry Unit, Jawaharlal Nehru Centre for Advanced Scientific Research, Jakkur, Bangalore 560064, India. E-mail: rv@jncasr.ac.in*
[b]*International Centre for Materials Science, Jawaharlal Nehru Centre for Advanced Scientific Research, Jakkur, Bangalore 560064, India*

† Electronic supplementary information (ESI) available. See DOI: https://doi.org/10.1039/d3nr03542e

In this work, we design a stable Cu, Mn dual-doped ZnSe QD system as a white light emitter using the robustness of dopant mid-gap states. We strategize the doping method in such a way that the dopants are incorporated in two distinct steps and are successfully doped in the same QD. While Mn is best doped using the nucleation-doping strategy,[18] Cu follows the growth-doping method.[19] A diffusion doping method[20] is employed to obtain small clusters of MnSe that are then diffused into the lattice during host growth at high temperature.[21] The chromaticity of the white light emission can be tuned by surface modification or by wavefunction modulation achieved by changing the extent of doping as well as host composition. The intensity of Cu emission to the band edge states is controlled by the number of surface hole trap states.[22–24] We study the effect of Cu to Mn states in the dual-doped QDs and obtain a rationale to tune the Commission International d'Eclairage (CIE) coordinates. We study the stability and color robustness as a function of temperature and exposure to UV excitation light. We change the host bandgap by alloying Cd into ZnSe and study the white light-based emission tunability from bluish white to orangish white for possible LED applications.

2. Results and discussion

Percentages of incorporated dopants and host cations were quantified using inductively coupled plasma optical emission spectroscopy (ICP-OES) measurement with Mn percentage at ~1–2%, Cu at less than 1%, and Cd^{2+} ions ranging from ~10% to 51%, tabulated in Table S1 in the ESI.† Characterizations of purified dual-doped QDs using X-ray diffraction (XRD) and transmission electron microscopy (TEM) are shown in Fig. S1 in the ESI.† Comparison of the XRD patterns with that of the bulk counterparts obtained from the ICSD database (Fig. S1a†) indicate the formation of cubic zinc blende structure, with a shift from ZnSe to CdSe with increasing Cd concentration demonstrating successful alloying of Cd. Broadening of XRD peaks confirms small particle size, consistent with TEM images of uniformly distributed spherical particles with an average size of 5 nm (Fig. S1b and S1c†). It is important to note that the size (size analysis is shown in the ESI Fig. S2a and 2b† respectively) does not increase upon Cd doping, marking the absence of any core/shell formation. HRTEM analysis reveals interplanar spacing of 3.33 Å ((111) plane) for ZnSe (inset to Fig. S1b†) and three major planes with *d*-spacing of 3.58 Å, 3.38 Å, and 3.05 Å for Cd alloying into the ZnSe lattice (inset to Fig. S1c†). The planes are marked as 'A', 'B', and 'C' in the Fourier transform (Fig. S1d†). The A and B planes nearly match with the (111) plane of cubic CdSe and ZnSe respectively and the C plane corresponds to the (200) plane of cubic CdSe.

Dual-doped ZnSe QDs were characterized optically using UV-visible and photoluminescence (PL) spectroscopy and a basic comparative study was done between QDs doped with individual dopants and dual-doped QDs. Fig. 1a shows the comparison plot of UV-visible spectra of singly-doped and dual-doped QDs. Cu-doped ZnSe shows a band edge absorption peak at ~3.27 eV while both Mn-doped ZnSe and dual-doped ZnSe show the same at ~3.0 eV. This is due to the different doping methods and nucleation temperature of ZnSe in Cu-doped ZnSe and MnSe in both Mn-doped ZnSe and dual-doped ZnSe QDs. In Fig. 1b, PL spectra of Mn-doped ZnSe consist of a purely characteristic orange emission at 2.12 eV arising from the $^4T_1 \rightarrow {}^6A_1$ transition of Mn^{2+} states. On the other hand, Cu-doped ZnSe shows a characteristic broad Cu emission peak at ~2.6 eV with blue-green emission along with the excitonic peak.[26] When we incorporate these two dopants together into the same ZnSe host, we observe a broad three-peak emission feature covering the entire visible spectrum. We then input the spectrum in a chromaticity diagram and obtained the CIE coordinates (0.31, 0.35) as shown in Fig. 1c which is closer to the standard WLE having CIE coordinates (0.33, 0.33). The decay profiles of Mn and Cu-related emission are presented in Fig. 1d and e respectively. Here, we have presented the dopant lifetime decay till two orders of magnitude because the data beyond this is not very reliable as it accounts for the dark currents. Decay dynamics of Mn emission in Mn-doped ZnSe QDs appear to be single exponential. However, the addition of Cu increases the lifetime of Mn emission drastically with an initial fast component in the system (fitting results shown in Table S2†). For example, the lifetime of spin-forbidden Mn emission in Mn-doped ZnSe is ~245 μs while it gradually increases to ~920 μs upon annealing for 60 minutes in the presence of Cu in dual-doped ZnSe QDs. Although Cu emission shows an increase in the slow component of the Cu lifetime (fitting results shown in Table S3†) in dual-doped QDs (τ_{avg} = 52 ns) it can be attributed to the overlap of the broad Mn emission at the Cu emission energy. However, a direct correlation is not possible due to several magnitudes of difference between the two lifetimes and the fast component in Mn emission is very near to the IRF of the excitation source.

The incorporation of two dopants created two competitive decay channels. It is by now well observed that the Mn emission occurs due to the ultrafast excitation of the Mn d-states from its ground state to the excited state.[27] While the exact mechanism of Mn d–d excitation has been debated and probed in several earlier reports,[28] here we acknowledge the need to have both the photogenerated hole (PGH) and the photogenerated electron (PGE) to excite the Mn d-states based on the previous studies in literature using femtosecond pump–probe techniques, photoluminescence excitation (PLE) and gated PLE measurements, *etc.*[27,29–31] However, on the other hand, Cu emission is driven by the host absorption and requires the presence of only a PGE to obtain a radiative emission. Thus, the efficiency of defect states in capturing the photogenerated hole determines the overall spectrum.[24] Further, it should be noted that the PL decay lifetime of Cu-doped ZnSe is known to be ranging from 30–50 ns similar to the literature reported earlier.[32] The lifetime of the Cu emission in Zn-based compounds is known to be lower compared to its cadmium compounds. While the exact reason for this

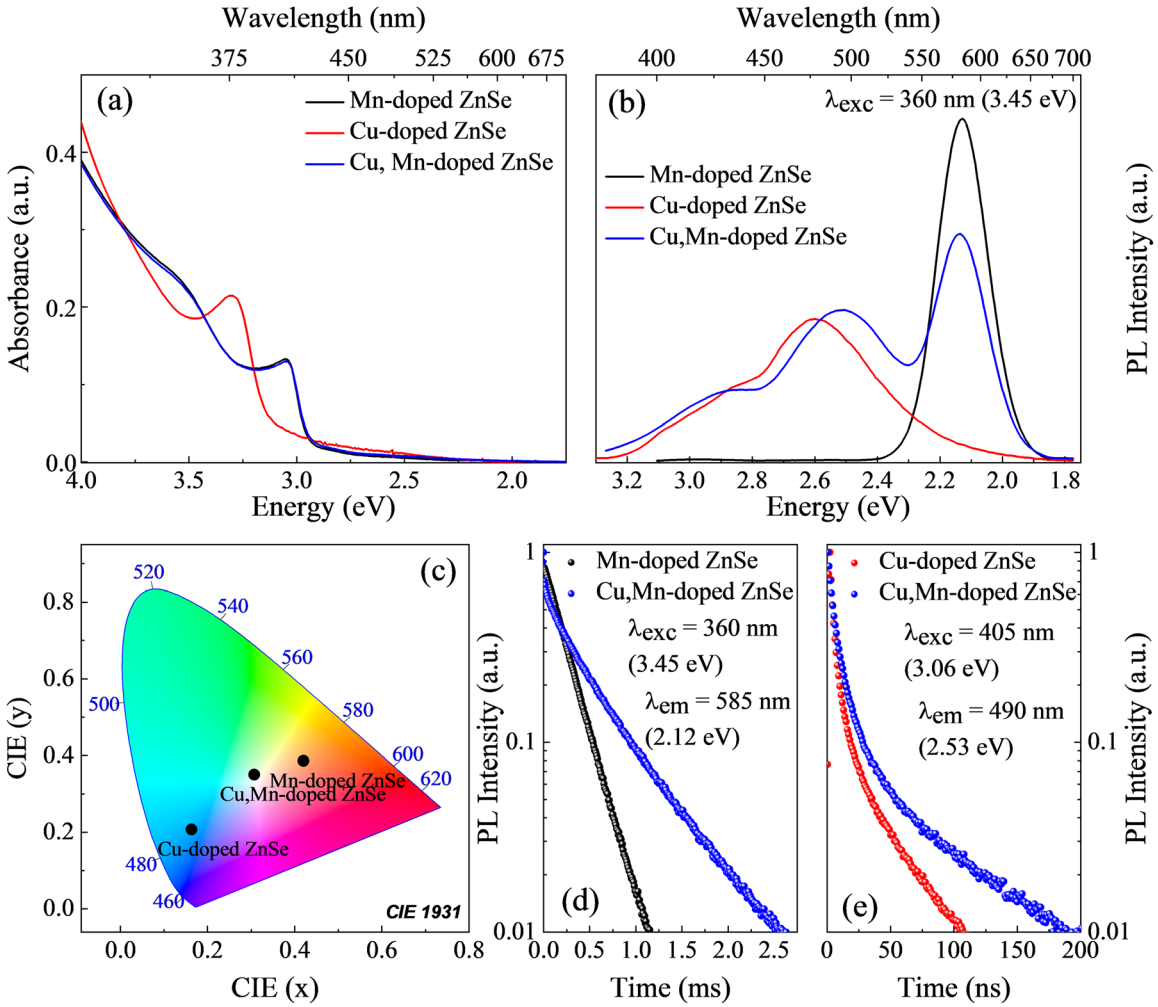

Fig. 1 Optical characterization of doped ZnSe QDs. (a) UV-visible, and (b) PL spectra of Mn-doped ZnSe (black), Cu-doped ZnSe (red), and Cu, Mn dual-doped ZnSe (blue). (c) Chromaticity diagram showing the CIE coordinates for individually doped as well as dual-doped ZnSe QDs. Comparative decay profile of (d) Mn emission and (e) Cu emission.

difference in lifetimes is yet to be understood, it could possibly be due to a better match in ionic radii of Cu^{2+} and Zn^{2+} and hence a better overlap. This further assists Cu in grabbing the photoexcited electron from the Mn. The fraction of charge carriers having yet longer lifetime that Cu is not able to draw will recombine through forbidden Mn d–d states resulting in a slower component in the Mn emission decay profile in the case of dual-doped system.

To confirm that both the dopants are incorporated in a single QD and that it is not a mixture of two individually doped QDs, we took the most conventional path by synthesizing Mn-doped ZnSe and Cu-doped ZnSe QDs individually followed by mixing them together. We then annealed the mixture for a period of 2 hours at a temperature as high as 180 °C. We chose the annealing temperature to be 180 °C because Cu is known to be expelled out of the QDs at higher temperature[26] and we judiciously avoided the loss of any dopant ions to retain the electronic structure intact during the annealing process. Few aliquots were collected at different time intervals during the annealing and their optical properties were measured. Steady state PL data were analyzed to track any changes during the process of annealing. The relative ratio of area under the two dopant emission peaks to the total area represents the relative probability of transition through the dopant channel and the same as a function of annealing time is shown in Fig. 2a. We compared the dual-doped QDs with that of the physical mixture containing two dopants and observed the probability transition variation over a period of several minutes of annealing for both the cases. The relative intensity of Cu and Mn emission remains unaltered in the case of physical mixture of doped QDs for as long as 120 minutes due to the absence of any dopant–dopant interaction. However, Cu emission intensity is seen to be increasing at the expense of Mn emission just within 15–30 min of annealing in the case of dual-doped QDs. This is due to the comparable ionic radii of Zn^{2+} and Cu^{2+}, where Cu^{2+} can efficiently replace host Zn^{2+}, and with annealing, more and more Cu^{2+} ions get incorporated. As explained before, Cu^{2+}

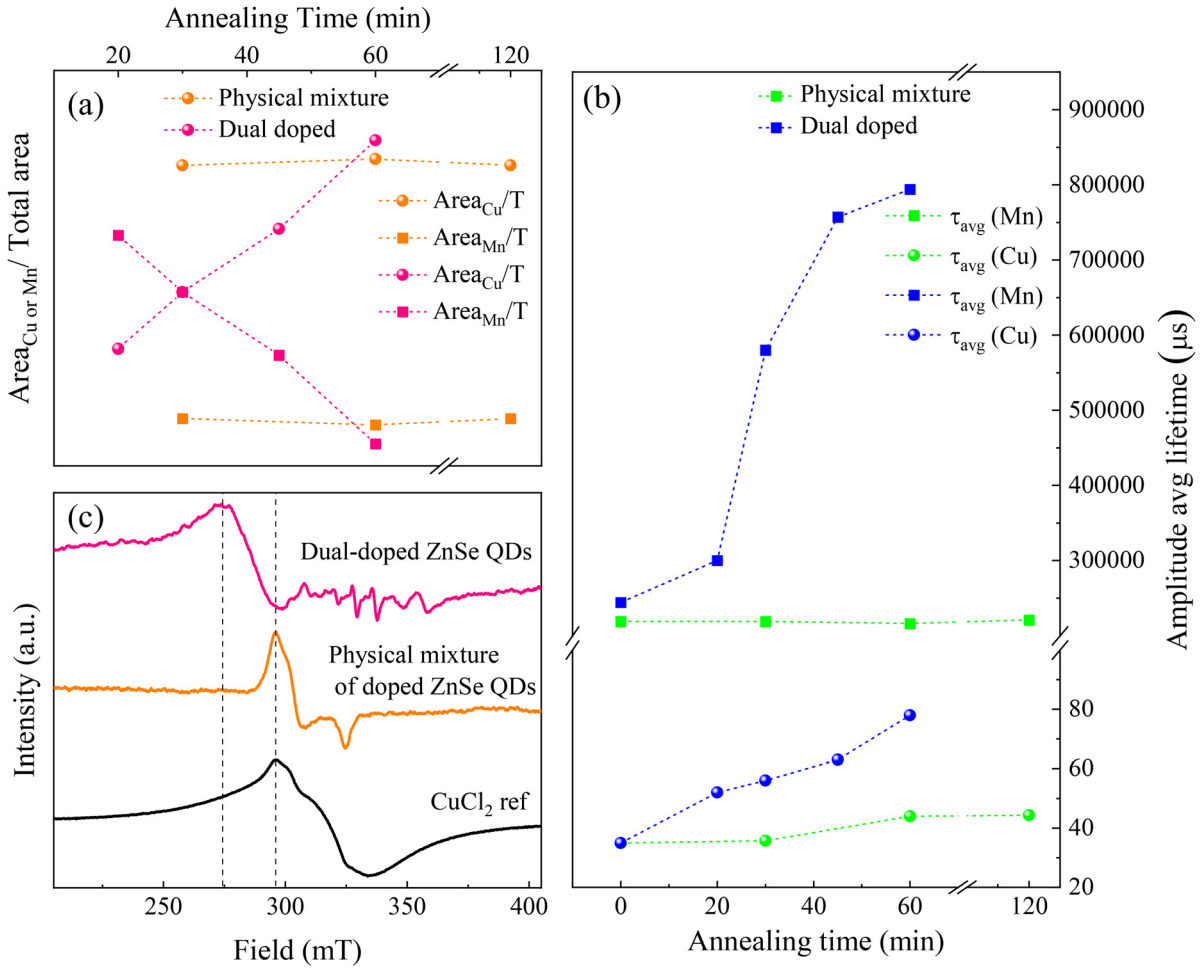

Fig. 2 (a) Relative ratio of area under dopant emission peaks (Cu in filled circles and Mn in filled squares) to the total area which quantifies the relative intensity ratio of dopant emission in case of both physical mixture of individually doped QDs and dual-doped QDs. (b) Amplitude-average lifetime of Cu (filled circles) and Mn (filled squares) emission of physical mixture of individually doped QDs and dual-doped QDs, and (c) EPR spectra of physical mixture of individually doped QDs (orange) and dual-doped QDs (pink) along with reference Cu salt.

extracts the back-transferred electrons from the host conduction band before they recombine through forbidden d–d states of Mn^{2+} giving rise to increased Cu PL intensity. In addition to that, time-resolved photoluminescence (TRPL) data shown in Fig. 2b reveals that the average lifetime of Cu and Mn emission show almost no change in the annealed physical mixture, while in the dual-doped QDs the Mn emission lifetime increases. This is in line with the increasing Cu emission intensity due to the more efficient decay through this channel. It should be noted that the photoexcited electron cannot be withdrawn from dopants present in two different dots confirming the inclusion of both the dopants in a single dot and not just merely mixed. The small increase in the Cu lifetime is attributed to the tail of the Mn emission occurring at that energy. Similarly, electron paramagnetic resonance (EPR) spectroscopic measurements were performed for both physical mixture of Mn–ZnSe and Cu–ZnSe QDs as well as dual-doped QDs, shown in Fig. 2c. Comparison of the EPR spectra suggests that in the case of physical mixture, no shift is observed in Cu EPR line as compared to $CuCl_2$ reference. However, a distinct Cu EPR line shift is observed in the case of dual-doped QDs suggesting an interaction between dopant ions in dual-doped QDs.[33]

Upon confirming the QDs to be dual-doped and the emission to be arising from a single source, we turn our attention to tuning of the color rendering. It is important to understand the electronic structure of the bulk and surface of the NCs and its effect on the transition dynamics of the different emission bands to modulate them in producing the white light to our demand. Hence, in the subsequent sections, we discuss the effects of relative concentration of the dopants as well as the other ligands to modulate the dopant emission.

Cu, when doped into the intrinsic QDs, is known to introduce a single atomic-like state in between the valence band (VB) and conduction band (CB) that alters the whole decay dynamics of the charge carriers.[34] Herein, we introduced Cu precursor in different stoichiometric ratios in the Mn-doped QDs, as shown in Fig. 3a. Inclusion of Cu in Mn-doped ZnSe

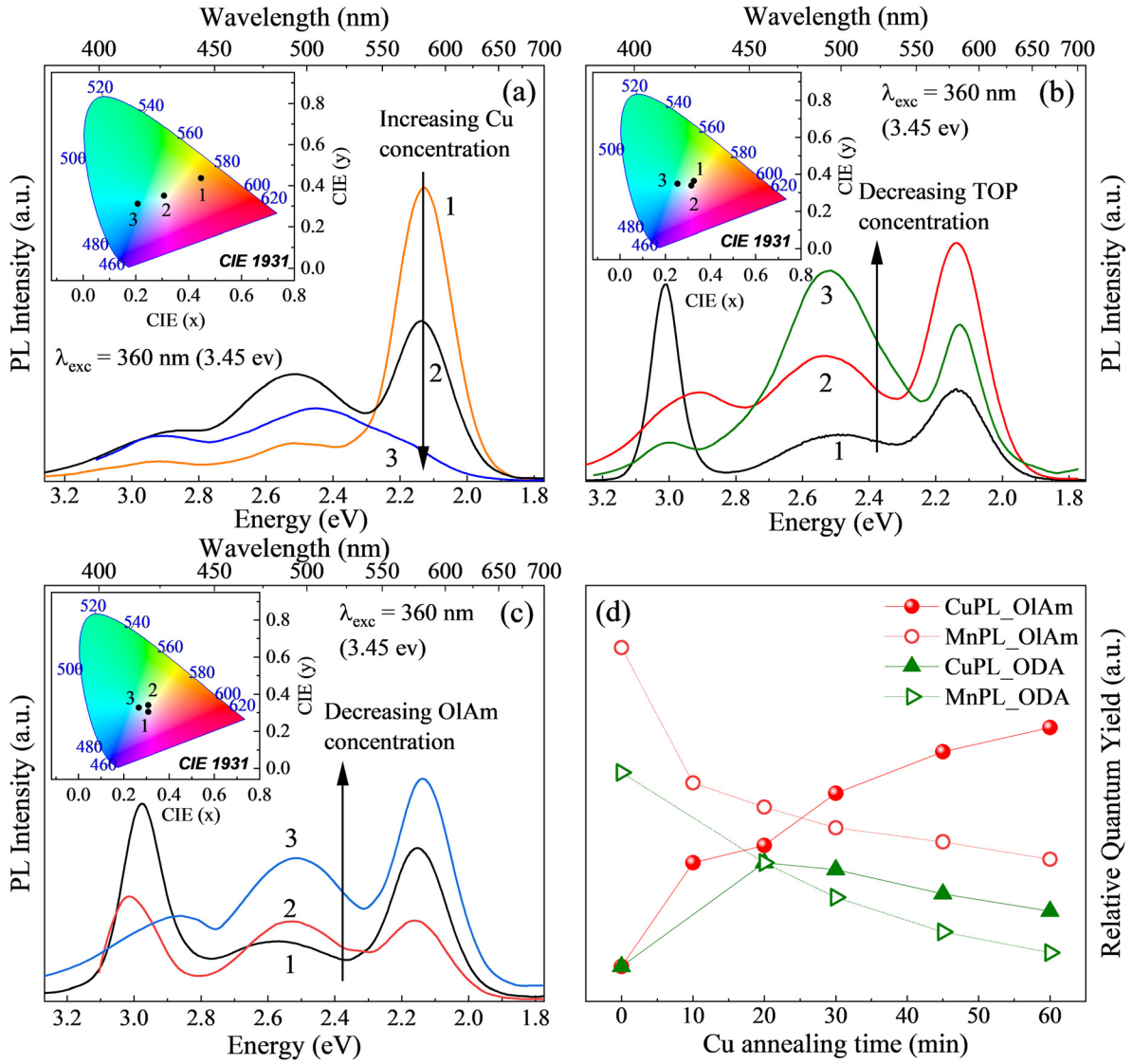

Fig. 3 PL spectra of Cu, Mn dual-doped ZnSe QDs as a function of (a) Cu concentration (b) TOP concentration, and (c) oleylamine concentration. Corresponding chromaticity diagrams are in the inset to the figures showing the variation in white light emission. (d) Relative quantum yield of Cu (filled shapes) and Mn-related (empty shapes) emission as a function of Cu annealing time when the dual-doped QDs were treated with oleylamine and octadecylamine.

QDs results in the appearance of a new blue-green emission band at around 2.50 eV (~495 nm) and with increase in the amount of Cu precursor we observe a steady increase of Cu emission intensity along with suppression of characteristic orange emission of Mn and the same is represented in the corresponding chromaticity diagram shown in the inset to Fig. 3a. The ICP-OES measurements reveal that the concentration of incorporated Cu remains almost constant, although we increase the stoichiometric percentage of the Cu precursor as shown in Table S4.† However, quantum yield (QY) results show that although the overall QY is initially maintained, upon an excess of Cu precursor, we observe a decrease in the QY as shown in Table S4.† These result points towards the fact that initially more QDs are doped with Cu. When almost the entire fraction of QDs get doped with Cu, further increase in Cu precursor leads to the excess Cu^{2+} ions being present at the surface (shallow trap states) which act as electron trap states (essentially the deficit of negative charge or excess positive charge that arises due to the under-coordinated cation in the crystal structure) and causes an overall reduction in the PL QY.

Trioctylphosphine (TOP) is proven to be a very good solvent for selenium as well as a good surface passivator of QDs, especially a good hole trap (excess negative charge arising due to the under-coordinated anion) passivator in CdSe QDs. However, in addition to being a hole trap passivator, it is also known to create electron traps at the surface of NCs due to the presence of a lone pair of electrons on the phosphorus atom in phosphine as observed from studying the Cu-doped

NCs.[22,23] This suggests the need to use TOP in moderation to increase the overall QY. However, within the range of suitable concentrations, one can use different concentrations to amplify the required dopant emission in the case of dual-doped QDs. Fig. 3b shows the PL spectra of QDs treated with different amounts of TOP while their respective QYs are given in Table S5.† When the highest amount of TOP is employed, we see more intense excitonic as well as Mn emission as compared to the Cu emission. However, due to new electron traps, the overall QY decreases. Analysis of the TrPL data (as shown in the Fig. S3†) of the nanocrystal systems shows an increasing contribution of the fast component with increasing TOP concentration. As explained in earlier literature[23] this very fast component in the TrPL data confirms the creation of electron trap states in nanocrystals. Upon varying the TOP amount, the emission dynamics of these three emission peaks change. The intensity of Cu emission gradually starts increasing while the other two reduce with respect to Cu with decrease in TOP concentration. These results suggest that TOP passivates hole traps present at the QD surfaces by getting attached to the undercoordinated selenium sites similar to the situation observed in Cu-doped NCs.[23] Thus, the QDs with TOP concentrations in the range from 0.25 mL to 0.5 mL retain high QY as well as assist in tuning the color of the white light emission as shown in the inset to Fig. 3b. CIE coordinates reveal that by varying the TOP concentration one can tune the electronic structure in such a way that different type of white light emission could be achieved. It is important to note here that TOP is used to treat only the QD surface and to the best of our knowledge, it does not affect the core electronic structure and Cu dopants being present at the core of QDs do not get affected by the TOP ligands. In fact, the highest amount of TOP is used in a 1 : 10 ratio to the entire reaction volume which acts only on surfaces and not in the core matrix.

The role of oleylamine is known to vary from system to system. For example, it passivates hole traps in CdSe QDs while it creates hole traps in CdS.[23] To examine the role of this amine further, we treated our dual-doped QDs with varying amounts of oleylamine, and the resulting PL spectra are shown in Fig. 3c. From the figure, we note that the dual-doped ZnSe QDs, treated with TOP and oleylamine exhibit a shift in BE emission peak with varying ligand concentration. This is attributed to the differing Strokes's shift arising from the different capping. It is well-studied in the literature that this Stokes shift is controlled by ligand–surface interactions and a strong vibronic contribution from surface states has a strong impact on the Stokes shift in colloidal QDs.[35–37] It cannot be attributed to any change in the size as the absorption spectra for all samples are very similar with identical band gaps as shown in Fig. S4.† Secondly, we observe that while the relative intensities of the Cu to Mn are very similar to that of TOP, overall QY remains largely constant with increasing oleylamine concentration in the reaction. This suggests that oleylamine acts as a hole trap for ZnSe QDs. Due to additional hole traps, PLQY of the band edge emission and Mn emission decreases. However, since the electron traps are relatively unaffected, the overall QY is retained as shown in Table S6,† changing only the chromaticity of the emission. A corresponding chromaticity diagram ranging from neutral white to cool white by changing the oleylamine concentration is shown in the inset to Fig. 3c. However, the role of amines is complicated and cannot be easily extrapolated to other amines as well as to other hosts. For example, we saw that the oleylamine creates hole traps but largely does not affect the electron traps, we observe very different behavior with the octadecylamine (ODA). We introduced the Cu dopant and annealed the sample for a long time and collected the samples at different intervals of time. The PL spectra collected at different time intervals for the two amines looked largely similar as shown in Fig. S5.† However, we observe a substantial change in the relative QY of the dual-doped samples as shown in Fig. 3d. Unlike oleylamine, in the case of ODA, the Cu emission grows at the cost of Mn emission only for the first 15 minutes of annealing. Subsequently, the overall QY of the sample decreases. Since oleylamine does not affect the electron traps, the overall QY remains constant, and as more Cu gets incorporated with increasing annealing time, we observe an intensification of Cu emission. However, in the case of ODA treatment, there is a drop in overall PLQY suggesting that ODA also creates electron traps along with creating hole traps.

Having optimized the ligand concentration, we study the effect of annealing time on the QY as well as the chromaticity of the NCs. Fig. 4a shows the contrast of Cu and Mn emission intensity which suggests that initially when the concentration of Cu dopants is less, Mn emission dominates and emits warm white light shown in corresponding chromaticity diagram in Fig. 4b. However, when large extent of Cu is incorporated, Cu emission starts dominating over yellow-orange Mn emission and nature of white light shifts from warm to neutral to cool white, marked from 1 to 7, as shown in Fig. 4b. Additionally, it was also observed that the overall QY changed very minimally after about 15 minutes of annealing providing a path to tune the chromaticity of the white light emission as shown in Table S7.†

Further two important parameters that play an important role in the effectiveness of the LED are its stability as a function of temperature and excitation light. Hence, we perform these two studies and the resulting PL spectra and relative QYs as a function of time are shown in Fig. S6 in the ESI.† From Fig. S6a,† it is evident that the relative QY of the white light emitting dual-doped QDs does not show any significant reduction with increasing temperature up to 350 K. Similarly, the QDs are significantly robust under continuous excitation and the QY is unaltered in the time frame of our study (up to 50 minutes) as shown in Fig. S6b.†

We then altered the host electronic structure by varying the composition of the host to achieve the variation of chromaticity with optimal QY. Since we have observed emission due to Cu dopants to be the dominating one in the optimal case, variation of composition will provide us further emission tunability starting from cool white to blue and up to orange. After the formation of white light emitting Cu, Mn dual-doped ZnSe

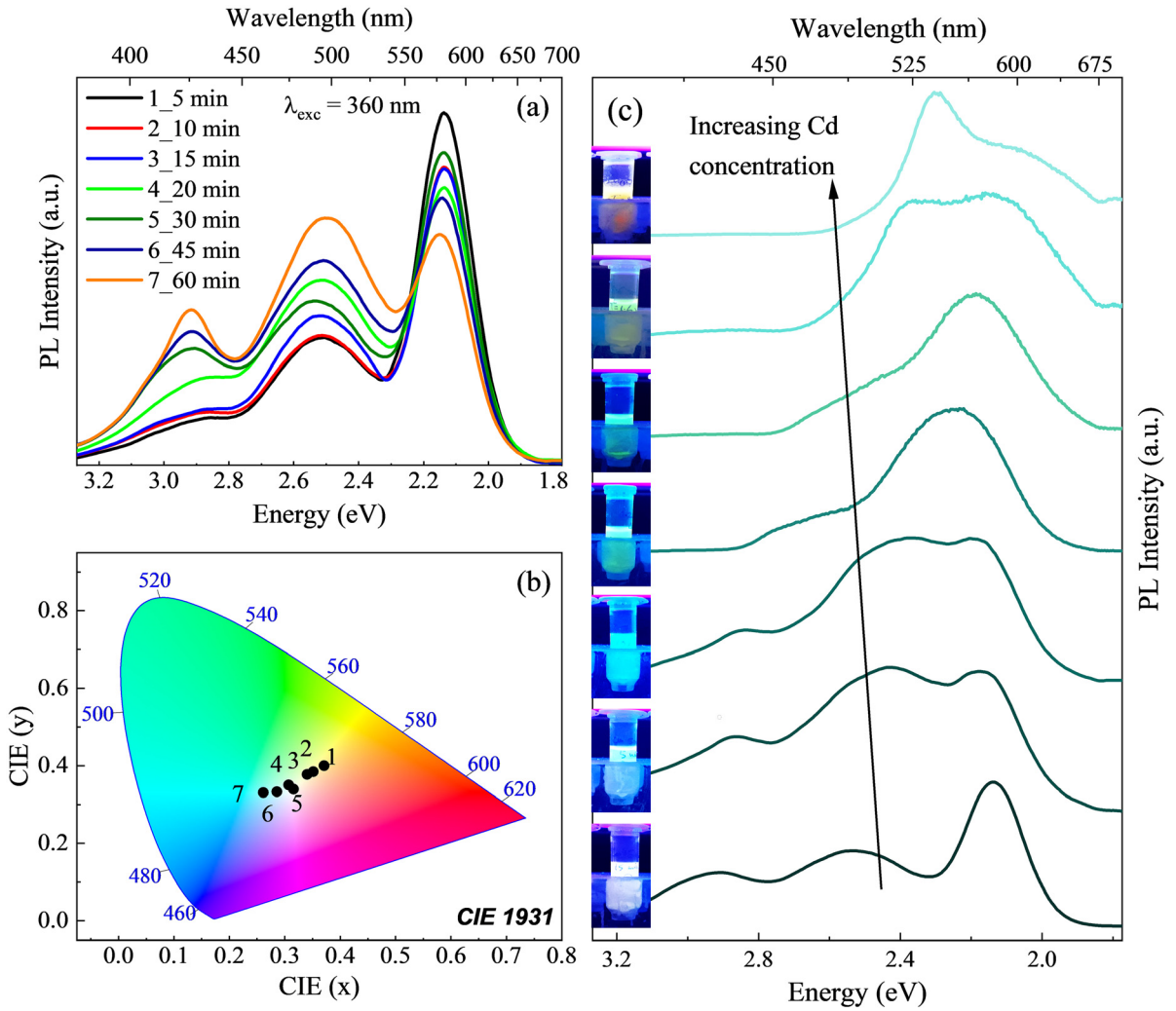

Fig. 4 (a) PL spectra of Cu, Mn dual-doped ZnSe QDs as a function Cu annealing time and, (b) corresponding chromaticity diagram shows the gradual shift in CIE coordinates from warm white to neutral white to cool white (c) evolution of steady state PL spectra with increasing Cd content.

QDs, we further incorporated Cd into the host to synthesize dual-doped alloyed $Cd_xZn_{1-x}Se$ QDs. The PL spectra of dual-doped $Cd_xZn_{1-x}Se$ QDs with increasing Cd concentration are shown in Fig. 4c and with an increase in the Cd concentration, we observe that the three-peak structure appears to be a single broad peak covering the entire visible spectrum. Corresponding digital images are shown next to each spectrum. The images show the white light emission in dual-doped ZnSe and further tunable colors ranging from blue to orange arising out of Cd alloying into dual-doped ZnSe QDs demonstrating the variation in chromaticity with good QY from a single chromophore. Based on our previous studies as well as literature reports on individual Mn and Cu-doped nanocrystals,[24,29,32,38,39] we know that the Cu-related emission occurs through the transition of a photogenerated electron to the Cu d-level having a lifetime of a few ns to μs. Similarly in Mn-doped QDs, an efficient transfer of photoexcited hole occurs to the Mn site giving rise to a transient Mn^{3+} state. This transient Mn^{3+} species then absorbs energy to form the spin-

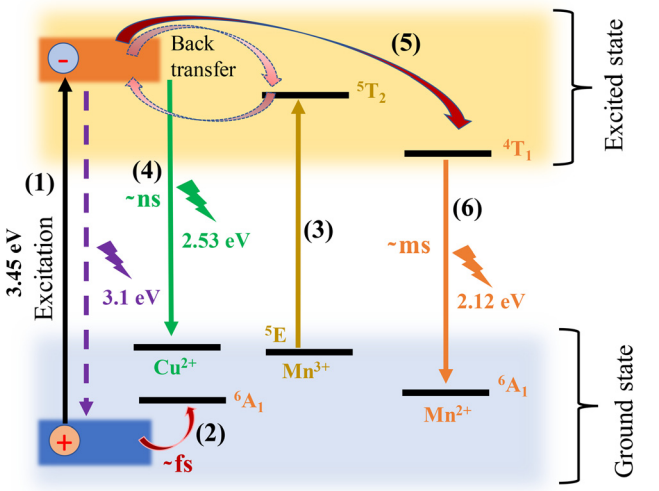

Fig. 5 Schematic representation of energy levels for Mn^{2+} and Cu^{2+} dual-doped ZnSe nanocrystals and the possible recombination pathways.

allowed $^5T_2$ state, which upon the capture of a photoexcited electron returns to the spin-forbidden excited $^4T_1$ state of Mn^{2+}, and photo-excited electron is later captured to reach a more stable Mn^{2+} state giving rise to the Mn emission involving ms timescale. Extrapolating these timelines from the singly doped nanocrystals to the dual-doped nanocrystals, and from their band structures, emission mechanisms, detailed recombination pathways, and their respective timelines, a schematic representation is shown in Fig. 5 explaining the possible pathways of charge carrier recombination and interaction between the energy states. However, detailed transient measurement studies on dual-doped nanocrystals can shed further light into the mechanism.

3. Conclusions

In conclusion, we proposed a facile and robust synthetic method for preparing white light emitting Cu, Mn dual-doped ZnSe QDs and synthesized the same and proved that the QDs are indeed doped with both the dopants simultaneously from various studies. We further explored the host electronic structure and the role of surface passivating ligands in altering the electronic structure in detail to attain very high reproducibility of the white light-emitting materials to meet the global demand for solid-state light sources. The white light-emitting device feasibility depends on color rendering index (CRI) and correlated color temperature (CCT).[40] An efficient white light-emitting material should have a high CRI and a CCT around 5000 K which is comparable to natural daylight.[41] In our work, we tuned the nature of white light from warm to neutral to cool white ranging the CCT from 3000 K to 7500 K. Accordingly, the CRI can also be tuned having varying white light emission efficiency. However, further tuning of the surface would be necessary to obtain an efficient electroluminescence for devices by avoiding the long chain non-conducting ligands on the surface without compromising on the luminescence. Nonetheless, it should be noted that the brightness is on par with other white light devices obtained from PL on blue emitting GaN LEDs.[15] Further, we altered the host electronic structure by incorporating another host component to attain tunable emission. Thus, we have synthesized a series of QDs with different types of white light emission as well as QDs with tunable emission ranging from blue to orange. These materials will be of great interest in the field of lighting applications, especially in light-emitting devices.

4. Experimental methods

4.1. Materials

Copper chloride ($CuCl_2$, 97%), elemental selenium, zinc stearate ($ZnSt_2$), zinc undecylenate ($ZnUt_2$), cadmium oxide (CdO), octadecylamine (ODA, 95%), oleylamine (technical grade, 70%), 1-octadecene (ODE, 90%), tributylphosphine (TBP), trioctylphosphine (TOP, 90%) were purchased from Sigma-Aldrich. Manganous chloride AR ($MnCl_2$), stearic acid LR were purchased from SD Fine chemicals, tetramethylammonium hydroxide pentahydrate (TMAH, 98%) was purchased from Spectrochem. Acetone, methanol, hexane, and toluene were purchased from Merck. All the chemicals and solvents were used as purchased without any further purification.

4.2. Synthesis of the precursors

Manganese stearate ($MnSt_2$) was synthesized by the method mentioned in the literature.[18] Briefly, stearic acid (20 mmol) was dissolved in methanol and added to TMAH solution of similar concentration, and stirred for 20 min. Meanwhile, 10 mmol manganous chloride was dissolved separately in methanol and added dropwise to the above-mentioned mixture with constant stirring. The appearance of a white precipitate shows the formation of $MnSt_2$. The solution was washed repeatedly with methanol followed by acetone. The white precipitate of $MnSt_2$ obtained was then dried in vacuum and used for further synthesis.

Copper stearate ($CuSt_2$) was prepared following the literature method.[25] Briefly, 10 mmol of stearic acid (SA) was dissolved in methanol and heated at 50 °C to get a clear solution. 10 mmol of TMAH was also dissolved in methanol separately and dropwise added to the SA-methanol solution. Meanwhile, 5 mmol of $CuCl_2$ was dissolved in methanol and slowly dropwise added to the above-mentioned solution under vigorous stirring. Sky blue precipitate of $CuSt_2$ was obtained and washed thoroughly followed by drying under vacuum.

Cadmium oleate ($CdOl_2$) was prepared by heating a mixture of 0.32 g of cadmium oxide, 7 mL oleic acid, and 9 mL of ODE to a higher temperature until the solution appeared colorless (~220–240 °C) under Ar atmosphere.

4.3. Synthesis of the doped QDs

Synthesis of Mn-doped ZnSe QDs. Mn-doped ZnSe NCs were synthesized following the nucleation doping method. Formation of MnSe nanoclusters is the most crucial step towards achieving Mn emission with high PLQY. The previously reported methods involved tributylphosphine-selenium compound as selenium precursor that not only restricts the reactivity of Se but also introduces toxicity due to the presence of unreacted tribuylphosphine. Herein, instead of organo-phosphine, we used elemental selenium as Se precursor with greatly controlled reactivity using an appropriate amount of oleylamine that results in a very fast and efficient formation of MnSe. Briefly, selenium powder (23.7 mg) and oleylamine (0.05 g) in ODE (5 mL) were loaded into a three-neck flask and degassed for 1 hour followed by bubbling with argon. The temperature was then raised to 280 °C. The manganese precursor solution (0.015 mmol $MnSt_2$ in 1 mL ODE) was then rapidly injected into the reaction flask at 280 °C. The reaction mixture was then allowed to cool to 260 °C for zinc overcoating with the injection of 0.5 mL of Zinc precursor solution (0.15 mmol of $ZnSt_2$ in 0.7 mL ODE), followed by injection of oleylamine to activate the zinc carboxylate. Temperature was further lowered to 240 °C and another 0.5 mL of zinc precursor (0.25 mmol of $ZnUt_2$ and 60 mg undecylenic acid in 1.4 mL

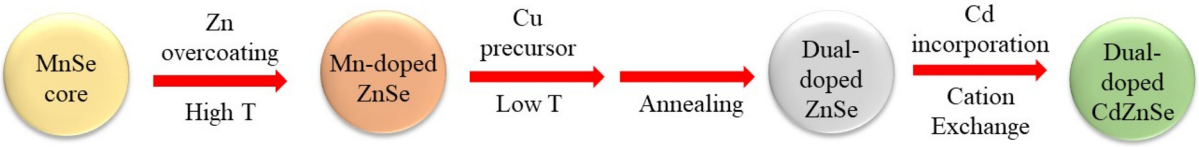

Scheme 1 Synthesis scheme involving nucleation and growth doping method for incorporation of Mn, and Cu into ZnSe lattice.

ODE) was injected after 10 min. The reaction flask was maintained at 240 °C for 10 min which was followed by injection of a designated amount of TOP. Finally, the reaction was allowed to cool down to room temperature, and the nanocrystals were washed using hexane and ethanol for further study.

Synthesis of Cu-doped ZnSe QDs. Cu-doped ZnSe NCs were synthesized following the growth doping method.[26] 0.1 mmol $ZnSt_2$ was taken in 5 mL ODE and the contents were degassed for an hour followed by purging with Argon. The temperature was then increased to 270 °C wherein Se precursor (1 mL TBP-Se in 0.5 g of ODA) was injected rapidly into the reaction mixture. The temperature was then set at 170 °C where Cu precursor was added. The reaction mixture was then annealed for 20–30 min at 190 °C followed by the addition of $ZnUt_2$ solution (0.12 g $ZnUt_2$ in 2 mL ODE). The reaction temperature was then increased to 210 °C for 10 min and finally reaction was allowed to cool down and purified using hexane and methanol.

Synthesis of Cu, Mn dual-doped ZnSe, and $Cd_xZn_{1-x}Se$ QDs. A general schematic for the synthesis of dual-doped nanocrystals is shown in Scheme 1. MnSe clusters are formed following a similar method discussed in the case of individual Mn-doped QDs. This is followed by overcoating with zinc precursor and then the addition of Cu and finally, cation exchange to synthesize dual-doped $Cd_xZn_{1-x}Se$ QDs. It should be noted here that nucleation and growth doping methods are decoupled to efficiently incorporate both Mn and Cu at two different stages of the reaction.

Briefly, Mn-doped ZnSe NCs were synthesized following the nucleation doping method already discussed in this work. Once the Mn-doped ZnSe QDs were formed, the reaction temperature was lowered to 180 °C, and a designated amount of Cu precursor was added. For Cu ions to get adsorbed onto the surface of QDs, the reaction temperature was raised to 210 °C and kept for 5 min and further reduced down to 180 °C followed by annealing for 30–45 minutes. This allows the Cu^{2+} ions to migrate inside from the surface resulting in the formation of Cu, Mn dual-doped ZnSe QDs.

Further, Cd alloying is done after reducing the reaction temperature further to 140 °C, and the gradual addition of $CdOl_2$ results in the formation of Cu, Mn dual-doped $Cd_xZn_{1-x}Se$ QDs. All the QDs were purified using hexane and methanol and used for further studies.

4.4. Characterization

The structure of the as synthesized nanoparticles was determined using the x-ray diffraction (XRD) technique on Rigaku Smartlab using Cu-Kα radiation and to get a high signal-to-noise ratio all patterns were recorded at a slow scan rate. Transmission electron microscopic (TEM) images were recorded using JEOL JEM-3010 transmission electron microscope with an accelerating voltage of 200 kV. Inductively coupled plasma optical emission spectroscopy (ICP-OES) was performed using PerkinElmer Optima 7000 DV instrument. Samples were prepared by washing the NCs to remove the excess precursors. Washed NCs were then digested in concentrated HNO_3 and diluted with Millipore water.

UV-visible absorption spectra of various aliquots dissolved in hexane were obtained using an Agilent 8453 UV-visible spectrometer. Steady-state PL spectra were collected using the 450 W xenon lamp as the source on the FLSP920 spectrometer, Edinburgh Instruments while the lifetime of Cu PL was measured using an EPL-405 pulsed laser, Edinburgh Instrument, and lifetime of Mn PL as well as gated PL measurements were carried out using microflash lamp.

Conflicts of interest

There are no conflicts to declare.

Acknowledgements

The authors thank JNCASR, Sheikh Saqr Laboratory and the Department of Science and Technology, Government of India, SERB-POWER Fellowship for financial support. PM and SD thank CSIR and INSPIRE respectively for fellowships.

References

1 A. L. Rogach, N. Gaponik, J. M. Lupton, C. Bertoni, D. E. Gallardo, S. Dunn, N. Li Pira, M. Paderi, P. Repetto and S. G. Romanov, *Angew. Chem., Int. Ed.*, 2008, **47**, 6538–6549.
2 H. V. Demir, S. Nizamoglu, T. Erdem, E. Mutlugun, N. Gaponik and A. Eychmüller, *Nano Today*, 2011, **6**, 632–647.
3 A. P. Alivisatos, *Science*, 1996, **271**, 933–937.
4 U. Resch-Genger, M. Grabolle, S. Cavaliere-Jaricot, R. Nitschke and T. Nann, *Nat. Methods*, 2008, **5**, 763–775.
5 P. Mondal and R. Viswanatha, *J. Phys. Chem. Lett.*, 2022, **13**, 1952–1961.

6 Q. Mo, C. Chen, W. Cai, S. Zhao, D. Yan and Z. Zang, *Laser Photonics Rev.*, 2021, **15**, 2100278.
7 D. Yan, Q. Mo, S. Zhao, W. Cai and Z. Zang, *Nanoscale*, 2021, **13**, 9740–9746.
8 S. Zhao, S. Jiang, W. Cai, R. Li, Q. Mo, B. Wang and Z. Zang, *Cell Rep. Phys. Sci.*, 2021, **2**, 100585.
9 P. O. Anikeeva, J. E. Halpert, M. G. Bawendi and V. Bulović, *Nano Lett.*, 2007, **7**, 2196–2200.
10 Y. Q. Li, A. Rizzo, R. Cingolani and G. Gigli, *Adv. Mater.*, 2006, **18**, 2545–2548.
11 A. Rizzo, M. Mazzeo, M. Biasiucci, R. Cingolani and G. Gigli, *Small*, 2008, **4**, 2143–2147.
12 M. A. Schreuder, K. Xiao, I. N. Ivanov, S. M. Weiss and S. J. Rosenthal, *Nano Lett.*, 2010, **10**, 573–576.
13 S. Sapra, S. Mayilo, T. A. Klar, A. L. Rogach and J. Feldmann, *Adv. Mater.*, 2007, **19**, 569–572.
14 C. C. Shen and W. L. Tseng, *Inorg. Chem.*, 2009, **48**, 8689–8694.
15 X. Yuan, R. Ma, W. Zhang, J. Hua, X. Meng, X. Zhong, J. Zhang, J. Zhao and H. J. Li, *ACS Appl. Mater. Interfaces*, 2015, **7**, 8659–8666.
16 S. K. Panda, S. G. Hickey, H. V. Demir and A. Eychmüller, *Angew. Chem., Int. Ed.*, 2011, **50**, 4432–4436.
17 A. Nurmikko, *Nat. Nanotechnol.*, 2015, **10**, 1001–1004.
18 N. Pradhan and X. Peng, *J. Am. Chem. Soc.*, 2007, **129**, 3339–3347.
19 B. B. Srivastava, S. Jana and N. Pradhan, *J. Am. Chem. Soc.*, 2011, **133**, 1007–1015.
20 A. Saha, A. Shetty, A. R. Pavan, S. Chattopadhyay, T. Shibata and R. Viswanatha, *J. Phys. Chem. Lett.*, 2016, **7**, 2420–2428.
21 A. Saha, M. Makkar, A. Shetty, K. Gahlot, A. R. Pavan and R. Viswanatha, *Nanoscale*, 2017, **9**, 2806–2813.
22 G. K. Grandhi, R. Tomar and R. Viswanatha, *ACS Nano*, 2012, **6**, 9751–9763.
23 G. K. Grandhi, M. Arun and R. Viswanatha, *J. Phys. Chem. C*, 2016, **120**, 19785–19795.
24 R. Viswanatha, S. Brovelli, A. Pandey, S. A. Crooker and V. I. Klimov, *Nano Lett.*, 2011, **11**, 4753–4758.
25 S. Sarkar, A. K. Guria, B. K. Patra and N. Pradhan, *Nanoscale*, 2014, **6**, 3786–3790.
26 D. Chen, R. Viswanatha, G. L. Ong, R. Xie, M. Balasubramaninan and X. Peng, *J. Am. Chem. Soc.*, 2009, **131**, 9333–9339.
27 H.-Y. Chen, S. Maiti and D. H. Son, *ACS Nano*, 2012, **6**, 583–591.
28 K. R. Pradeep and R. Viswanatha, *APL Mater.*, 2020, **8**, 020901.
29 K. Gahlot, K. R. Pradeep, A. Camellini, G. Sirigu, G. Cerullo, M. Zavelani-Rossi, A. Singh, U. V. Waghmare and R. Viswanatha, *ACS Energy Lett.*, 2019, **4**, 729–735.
30 H.-Y. Chen, T.-Y. Chen and D. H. Son, *J. Phys. Chem. C*, 2010, **114**, 4418–4423.
31 R. Viswanatha, J. M. Pietryga, V. I. Klimov and S. A. Crooker, *Phys. Rev. Lett.*, 2011, **107**, 067402.
32 S. Jana, B. B. Srivastava, S. Acharya, P. K. Santra, N. R. Jana, D. D. Sarma and N. Pradhan, *Chem. Commun.*, 2010, **46**, 2853–2855.
33 B. L. Bales, M. Meyer and M. Peric, *J. Phys. Chem. A*, 2014, **118**, 6154–6162.
34 P. Mondal, S. Chakraborty, G. K. Grandhi and R. Viswanatha, *J. Phys. Chem. Lett.*, 2020, **11**, 5367–5372.
35 T. G. Mack, L. Jethi and P. Kambhampati, *J. Phys. Chem. C*, 2017, **121**, 28537–28545.
36 L. Jethi, T. G. Mack, M. M. Krause, S. Drake and P. Kambhampati, *ChemPhysChem*, 2016, **17**, 665–669.
37 L. Jethi, T. G. Mack and P. Kambhampati, *J. Phys. Chem. C*, 2017, **121**, 26102–26107.
38 P. Mondal, S. Sathiyamani, K. Gahlot and R. Viswanatha, *J. Phys. Chem. C*, 2021, **125**, 11007–11013.
39 A. Dutta, R. Bera, A. Ghosh and A. Patra, *J. Phys. Chem. C*, 2018, **122**, 16992–17000.
40 G. C. Adhikari, S. Thapa, H. Zhu, A. Grigoriev and P. Zhu, *J. Phys. Chem. C*, 2019, **123**, 12023–12028.
41 M. Worku, Y. Tian, C. Zhou, S. Lee, Q. Meisner, Y. Zhou and B. Ma, *ACS Appl. Mater. Interfaces*, 2018, **10**, 30051–30057.